Journal of Materials and Environmental Science
ISSN : 2028-2508
e-ISSN : 2737-890X
CODEN : JMESCN
Copyright © 2026,

J. Mater. Environ. Sci., 2026, Volume 17, Issue 3, Page 424-434

http://www.jmaterenvironsci.com

Neem mediated SnO_2 nanorods: Influence of Thickness on the Optical Properties

Omoniyi F. O.*, Omoteji I. B., Imalerio T. I., Komolafe B. G., Babalola O. A.

Department of Materials Science and Renewable Energy, Physics Advanced Research Centre, SHESTCO, Kwali, Abuja, Nigeria

**Corresponding author, Email address: omoniyifrancis@gmail.com*

Received *01 Nov 2025,*
Revised *02 Mar 2026,*
Accepted *05 Mar 2026*

Citation: *Omoniyi F. O., Omoteji I. B., Imalerio T. I., Komolafe B. G., Babalola O. A. (2026) Neem mediated SnO_2 nanorods: Influence of Thickness on the Optical Properties, J. Mater. Environ. Sci., 17(3), 424-434*

Abstract: Abstract: In this paper, we studied the influence of thickness on the optical properties of the thin films of green-synthesized SnO_2 nanoparticles. Green synthesis is a cheap and eco-friendly method of material. Fresh neem extract and tin (II) chloride dihydrate aqueous solution were heated at 80 °C for 1 hour and the precipitate was filtered, dried and annealed at 400 °C for 2 hours. The annealed SnO_2 was characterized for morphology with Scanning Electron Microscope (SEM), structural and crystallinity with X-ray Diffractometer (XRD), and optical properties with Ultraviolet Visible Spectrophotometer. Structural analysis confirmed a tetragonal phase, with crystallite size estimated using the Debye–Scherrer equation. SEM revealed nanorod-shaped particles ranging from 181.5 nm to 2.055 µm. Optical studies of films (4.8, 4.9, and 6.0 µm) showed thickness-dependent band gaps of 3.14, 3.37 and 3.49 eV. The refractive index decreased from about 1.5 (thinner films) to about 1.1 for 6 µm thickness. The optical property revealed the optimal threshold thickness as 4.9 µm and the applications as anti-reflective coating and photovoltaic absorber. The estimated Urbach energy values showed the disorderliness in the 4.8 µm thick film by its 1,666 meV value compared to 945 meV of 4.9 µm thick film while, 6.0 µm thick film was insulative.

Keywords: *Nanorods; Neem extract; Tin dioxide; Optoelectronics; Sensor*

1. Introduction

The spontaneous increase in the research of nanoscience (Shim *et al*., 2015) has greatly impacted various research fields such as medical, environmental, solar energy, and pharmaceutical industries. These are where metal-based nanoparticles (NPs) are being used as an efficient material compared to their bulk counterparts (Miri *et al*., 2018; Sutjaritvorakul and Chutipaijit, 2018). The global demand for energy has driven the development of semiconductor oxide thin-film solar cells, which aim to efficiently convert solar energy (Babalola *et al*., 2024). One of the determinants of the applications of a semiconductor is the energy band gap. The energy band gap of semiconductors lies between the valence and the conduction band (Chaves *et al*., 2020; Kumar *et al*., 2020), which determines how easily electrons can be excited by light to reach the conduction band. Photo-induced effects have been reported to reduce the energy band gap by altering the conductivity of semiconductors, by excitation of electrons to high energy levels thus, increasing the charge current density (Drozdowska *et al*., 2022). Researches on the potential applications of semiconductor oxides such as Zinc Oxide (ZnO) for solar film are tremendous with ZnO having energy band gap of 3.37 eV at ambient temperature (Chen *et al*., 2018). Also, SnO_2 semiconductor was found suitable for energy storage theoretically due to its safety

and cheap production (Liu *et al*., 2019; Li *et al*., 2020). Nevertheless, the poor conductivity and ion diffusion of SnO_2 has limited its electrochemical performance (Park *et al*., 2008). Preparation of SnO_2 ink by Shen (2012) was by dissolving $SnCl_2{\cdot}2H_2O$ in alcohol. Deposition techniques such as spray pyrolysis (Eqbal and Anila, 2021), spin coating (Medas *et al*., 2025), inkjet printing technique and atomic layer deposition methods, have been used. Billur *et al*. (2020) reported the decrease in the transmittance of SnO_2 with increase in the thickness of films, and direct band gap between 3.8 eV and 3.9 eV, using inkjet printing technique to vary the thickness. Another recent work extrapolated direct band gaps between 3.91 and 4.03 eV (Bitu *et al*., 2023).

Green synthesis at low temperature is a new way for nanoparticles, because of its non-toxic and economical values (Oyelade *et al*., 2025). Research has shown the antimicrobial inhibition of SnO_2 on bacteria like *Escherichia coli* (*E. coli*) and *Klebsiella pneumonia* (*K. pneumonia*) and *Staphylococcus aureus* (*S. aureus*) (Haq *et al*., 2021). It is an n-type semiconductor and of importance, due to its optimal transparency in the visible region, strong adsorption property and low thermal stability. It is commonly known to have wide energy band gap of about 3.6 eV (Habte *et al*., 2022). The applications are found in optoelectronic devices, electrodes for lithium-ion battery, transistors, heat mirrors, protective coatings, solar cells and sensor for gases (Habte *et al*., 2022). Neem tree is known to be a medicinal tree for antimalarial among other applications. The extract has energy band gap of about 1.76 eV. The extract like any other plant extract also, has application in biosynthesis of metal nanoparticles and metal oxides. The phytochemicals of neem extract analyzed by Ali *et al*., (2022), identified Azadirachtin (a Limonoid), flavonoids, saponins, tannins, phenols and terpenoids using authentic standards procedures. The phytochemicals have carbonyl and hydroxyl functional groups as shown in **Figure 1**.

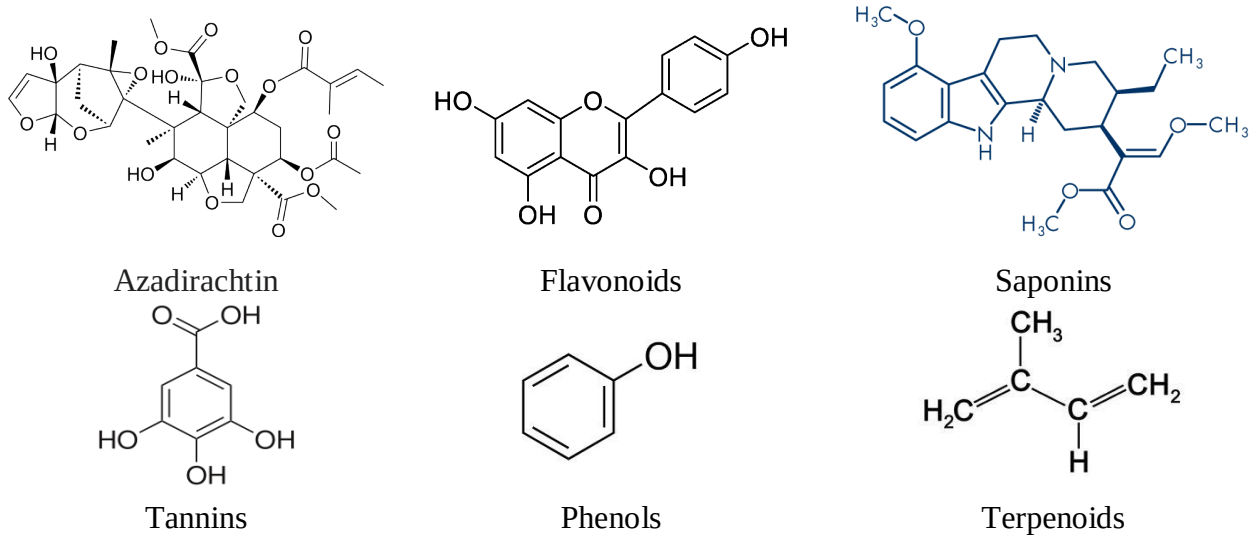

Figure 1. Structural diagram of Neem extract Phytochemicals

In this paper, we report a cheap synthesis and properties of tin dioxide using neem extract by examining the thickness of films for optoelectronics application.

2. Methodology

2.1 Materials

Tin (II) chloride dihydrate ($SnCl_2.H_2O$) obtained from PROLABO, and fresh Neem leaves that were collected.

2.2. Extraction process of Neem

Fresh neem leaves were collected and washed thoroughly with distilled water. A sizeable 10 grams of the leaves were weighed; soaked in 100 ml of distilled water in a 200 ml beaker, and heated at about 80 °C for 30 minutes. The temperature was allowed to drop to that of the room then, filtered with Whatmann filter paper. The neem extract was then used immediately.

2.3. Synthesis of Neem mediated SnO_2

An aqueous solution of $SnCl_2.H_2O$ was prepared by dissolving 10 grams of $SnCl_2.H_2O$ in 100 ml of distilled water. The aqueous solution was mixed with the neem extract gotten and heated at 80 °C for 1 hour. The residue formed was washed thrice and annealed at 400 °C for 2 hours. The nanoparticles formed, was further subjected to characterization and the slurry made from it was deposited on glass substrate using doctor blade method:

$$\text{Neem extract} + SnCl_2.H_2O \rightarrow SnO_2 \text{ complexes} + 2HCl \quad (*)$$

2.4. Characterization

2.4.1. Structural Characterization

The X-ray diffraction (XRD) was done with Tongda 3500 equipment, voltage of 40 KV, and 20 mA current, in step of 0.02°. The machine works with Bragg's principle related to Equation 1.

$$n\lambda = 2d\sin\theta \quad (1)$$

where n = integer representing order of reflection, λ = wavelength, d = spacing between atomic plane, θ = diffraction angle.

The crystallites sizes were determined using Debye-Scherer formula in Equation 2.

$$D = k\lambda/\beta\cos\theta \quad (2)$$

Where D is the growth, k which was assigned 0.94, λ is the X-ray wavelength of 0.15406 nm, β is the full width at half maximum (FWHM) in radians, and θ is the Bragg's angle.

The lattice parameter, $\boldsymbol{a}$, was calculated using Equation 3.

$$a = d\sqrt{(h^2 + k^2 + l^2)} \quad (3)$$

The produced radius, r, of the SnO_2 NPs is obtained using Equation 4.

$$r = (a\sqrt{2})/4 \quad (4)$$

2.4.2. Morphology Characterization

The scanning electron microscopy (SEM) was done using ZEISS EVO 10 machine with magnification of 2.04KX. The morphology revealed the nanorods shape of the nanoparticles, with various grains sizes.

2.4.3. Optical characterization (UV-Vis-IR)

The Ultraviolet Visible-Infrared (UV-Vis-IR) spectroscopy was done in the wavelength range of 200 nm to 1100 nm with aid of Filmetrics F10-RT-UV machine.

By Beer-Lambert law:

$$A = \log_{10} (I_o/I) \quad (5)$$

$$I = I_o e^{-ax} \quad (6)$$

$$\alpha = (2.303 \times A)/l) \quad (7)$$

where $\boldsymbol{\alpha}$ = absorption coefficient, I = intensity of transmitted light, I_0 = intensity of incident light, l = optical path length, A = absorbance.

The optical spectra analysis was determined by calculating the direct band gap with Equation 8:

$$(\alpha h\upsilon) = \beta(h\upsilon - E_g) \quad (8)$$

$\boldsymbol{\alpha}$ = absorption coefficient, $\boldsymbol{h\upsilon}$ = energy of the incident photon, $\boldsymbol{\beta}$ = constant, and $\boldsymbol{E_g}$ = band gap.

The optoelectronic property was determined by finding the Urbach energy using Equations 9 and 10 below:

$$\alpha = \alpha_o \exp(h\upsilon/E_U) \quad (9)$$

Taking the natural logarithm of Equation 9, we will have Equation 10.

$$\ln \alpha = \ln \alpha_o + (h\upsilon/E_U) \quad (10)$$

where 'E_U' = Urbach energy, 'α' = the absorption coefficient and '$h\upsilon$'= photon energy.

The refractive indices were estimated with Equation 11

$$n = (1 + \sqrt{R})/(1 - \sqrt{R}) \quad (11)$$

3. Results and Discussion

3.1. Chemistry of the Synthesis

The chemistry between $Sncl_2.2H_2O$ and Neem extract occur in phases such as hydrolysis, interaction with Neem extract, and the formation of SnO_2. The Neem biomolecules reduced, nucleated, and stabilized $Sn(OH)_2$ to SnO_2, which are capped by phytochemicals.

i. Hydrolysis: When the $Sncl_2.H_2O$ was dissolved in distilled water, which made it partially hydrolyzed as stated in Equation 12.

$$SnCl_2.2H_2O \leftrightarrow Sn^{2+} + 2Cl^{-} + 2H_2O \quad (12)$$

ii.$SnCl_2.2H_2O$ interaction with Neem Extract: Flavonoids and Polyphenols (-OH) are biomolecules that interacted with $SnCl_2.2H_2O$, and reduced it when heated. Polyphenols donate electrons, oxidizing themselves to quinone-like structure. The Sn^{2+} ions are oxidized to Sn^{4+} and precipitated as tin hydroxide ($Sn(OH)_2$) (Waris *et al*., 2021), which after annealing precipitated further to SnO_2. The precipitate is capped by phytochemicals :

$$Sn^{2+} + \text{Polyphenol (reduced form)} \rightarrow Sn^{4+} + \text{Polyphenol (oxidized form)} \quad (13)$$

iii. Formation stage: The Sn^{4+} in Equation 13 is in the form of $Sn(OH)_2$ which turns to SnO_2 after annealing.

$$Sn(OH)_2 \rightarrow SnO_2 + H_2O \quad (14)$$

3.2 X-ray diffraction (XRD)

Figure 2 showed the XRD of the synthesized Tin dioxide (SnO_2), revealed the major diffraction peaks at 26.58°, 33.87°, 37.95°, 51.77° and 54.75°, corresponding to (110), (101), (200), (211) and (220) Miller index respectively. These peaks were identified with the JCPDS number 72-1147 with tetragonal shape. The average of the crystallite sizes and radii were 14.450 nm and 0.158 nm. The average lattice parameter 'a' was 0.4470 nm.

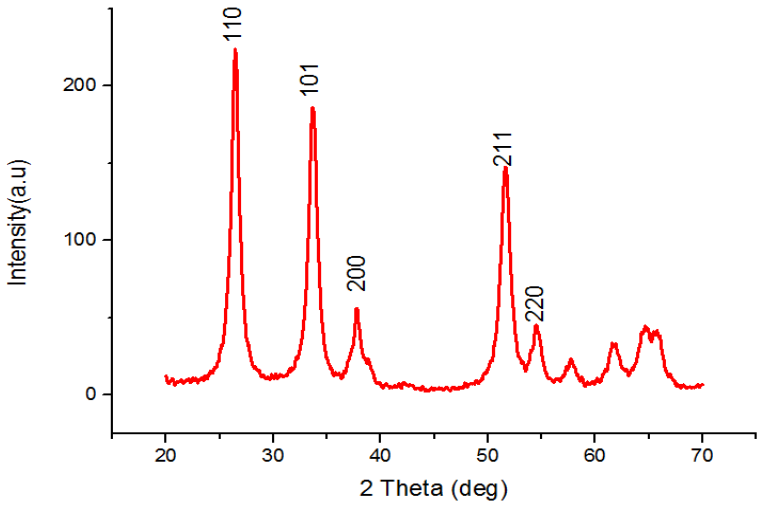

Figure 2. Diffractogram of SnO_2

Table 1: XRD analyses of SnO_2

2-Theta	Count	β (°)	β (rad)	d(nm)	hkl	D (nm)	(nm)*a*	r(nm)
26.58	198	0.609	0.0106	0.3368	110	14.036	0.4763	0.1684
33.87	150	0.673	0.0117	0.2653	101	12.937	0.3752	0.1327
37.95	33	0.592	0.0100	0.2379	200	15.312	0.4758	0.1682
51.77	113	0.708	0.0124	0.1766	211	12.980	0.4326	0.1529
54.75	38	0.552	0.0096	0.1680	220	16.985	0.4752	0.1680
					Average	**14.450**	**0.4470**	**0.1580**

3.2. Morphology

The result of the scanning electron microscopy (SEM) in **Figure 3** showed the morphology of the synthesized nanoparticles to be nanorods. The grains sizes ranged from nano to micron sizes. The measured grains in length using the SEM were within the range of 181.5 nm and 2.055 µm. The energy dispersive X-ray spectroscopy (EDX) showed the elemental composition in percentages.

3.3. UV-Visible spectroscopy

The UV-Vis spectroscopy of deposited tin dioxide of thickness 4.8 µm, 4.9 µm and 6.0 µm on glass substrates were analyzed. In **Figure 4A**, the figure demonstrated that all films are UV absorbers; the optical absorption strongly depends on film thickness. According to Özmenteş, 2025, transmittance should decrease with thickness but, reverse is the case between 4.8 and 4.9 µm in this work. This could only be caused by level of disorderliness of SnO_2 particles in the films resulting in varied transmittance.

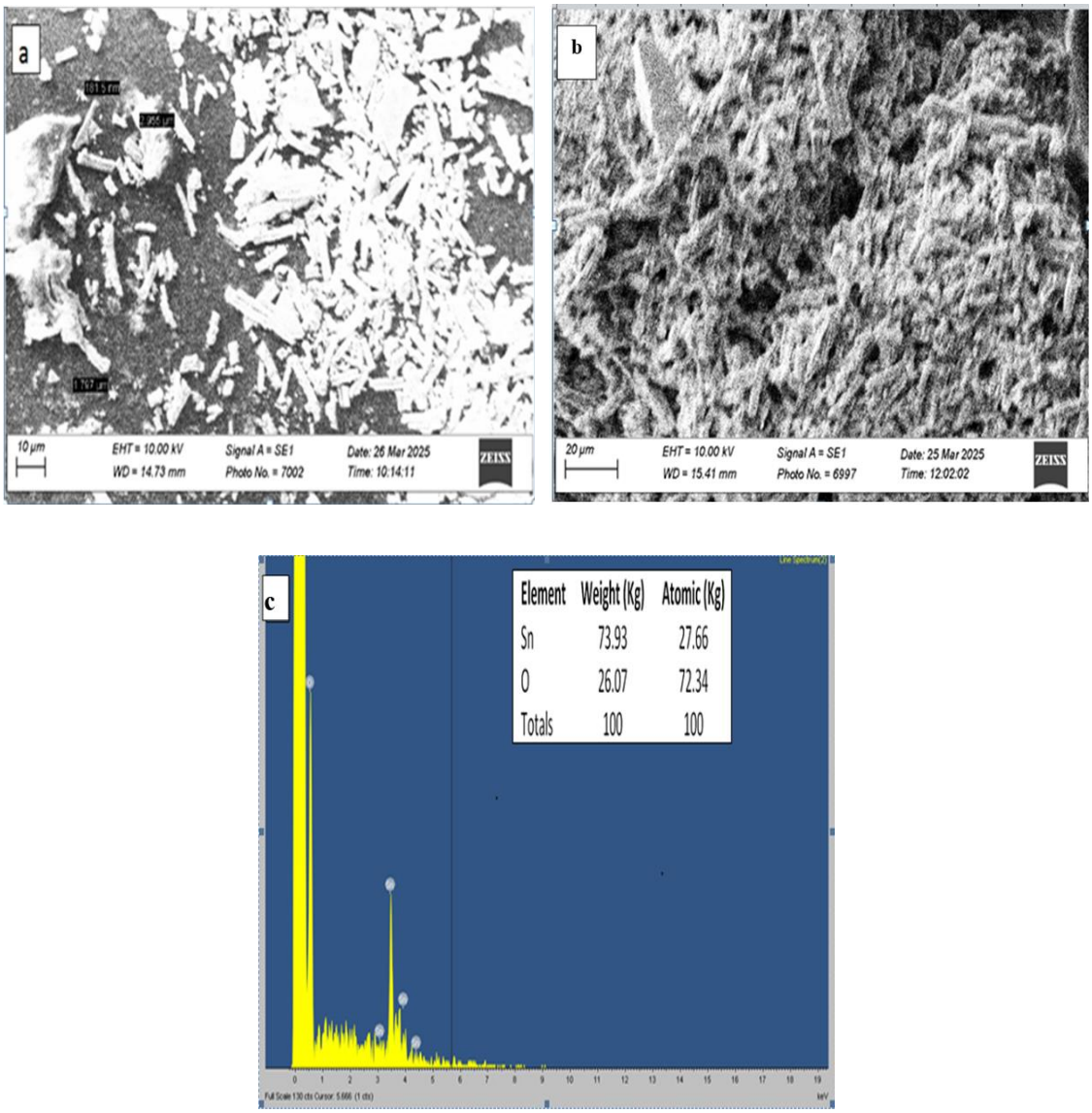

Figure 3. SnO_2 (a) Micrograph at 2.04 KX (b) Micrograph at 1.87 KX (c) EDX

The energy band gap increased with thickness thus, agreed with other works (Özmenteş, 2025; Omoniyi *et al*., 2025). The 4.9 µm film indicates the optimum threshold of thickness, balancing crystallinity and absorption efficiency whereas, the 6.0 µm film suffers from defect-induced absorption and poorer optical quality. This implies that, increasing film thickness beyond an optimum introduces more disorder, tail states, and scattering, reducing optical transparency (Ghasemi *et al*., 2022). **Figure 4B** showed the energy band gaps of 3.14 eV, 3.37 eV and 3.49 eV respectively with 4.8, 4.9, and 6.0 µm. The band gaps have reduced values when compared to 3.6 eV obtained by Habte *et al*., 2022 and that of other methods but, similar to the pattern obtained by Omoniyi *et al*., 2025 for lead oxide. The films exhibited transition in the energy gap. The thickness of 4.9 µm displayed optimum optical property with sharp edge while the value for 6.0 µm thickness is the least, and it is due to disorderliness of particles. The high transmittance of 4.9 µm was due to reduced disorderliness of SnO_2 in the film when compared to that of 4.8 µm. **Figure 4C** showed that, the film thickness of 4.9 µm transmitted about 36.4%, which is higher than that of 4.8 µm (23.7%) and 6.0 µm (1.7%). The reflectance of the thicknesses 4.8 µm and 4.9 µm are close while, 6.0 µm thick film had the least reflection, as shown in **Figure 4D**. The reduced energy band gaps were obtained by extrapolating the linear part of the plot. The potency of the green synthesis reduced the band gaps, to give a better result than those of other

synthesis methods (Billur *et al*., 2020; Bitu *et al*., 2023). The low transmittance was due to the thickness used unlike, films that were hundreds of nanometers thick. The low transmittance and reflectance indicated anti-reflectance property of SnO_2, and these enhanced the suitability of SnO_2 as photovoltaic absorber. **Figure 4A** thin films (4.8 and 4.9 µm) showed sharper band edges, while the 6.0 µm film showed absorption dominated with defect (less clear edge, flat absorbance).

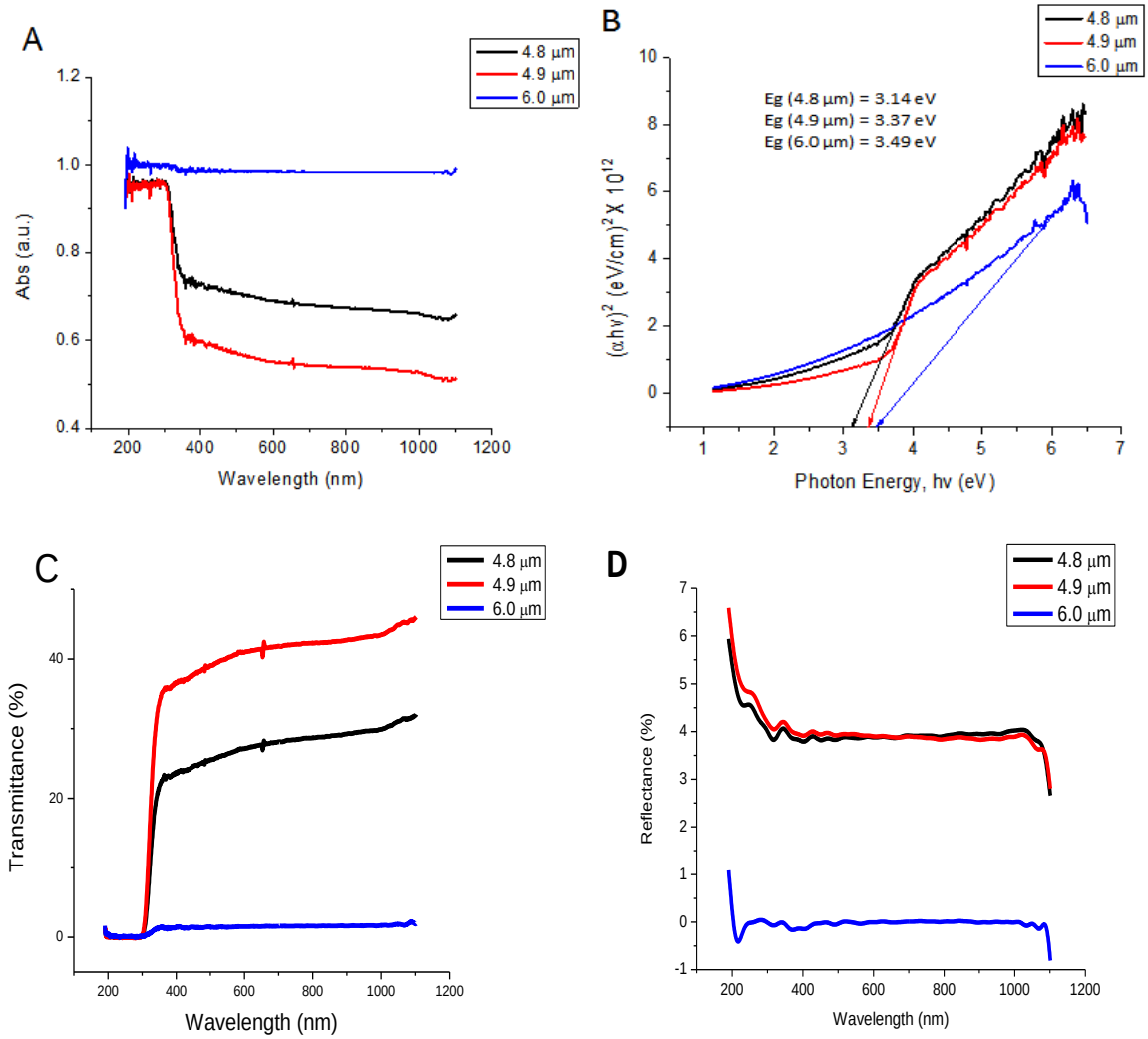

Figure 4. SnO_2 (A) UV-Vis-IR plot (B) Tauc Plot (C) Transmittance plot (D) Reflectance plot

Figure 5 showed all samples to exhibit strong absorption in the UV range, which is typical of semiconductor/oxide thin films. This indicates that the films have wide band gaps, absorbing mainly in the UV (Rafee *et al*., 2025). For semiconductors, the sharp absorption edge corresponds to the band gap energy within the UV wavelength around 350–400 nm. The 4.8 µm thick film showed relatively high absorption in UV, gradually decreasing in visible and NIR regions. The 4.9 µm thick film also absorbed strongly in UV but, showed the steepest drop in absorption after about 400 nm, maintaining the lowest absorption in visible and NIR. The absorption curve of 6.0 µm thick is flatter and almost constant after 400 nm, suggesting more defect-related or scattering rather than band-to-band absorption. The 6.0 µm thick film had the highest energy band gap as well as lower UV absorption compared to 4.8 and 4.9 µm (Kumar *et al*., 2011). This shows that, increasing thickness will introduce more structural defects, disorder, or scattering that reduces effective optical absorption. Thickest film (6.0 µm) showed degraded optical quality showing that, increasing film thickness beyond an optimum value reduces the optical quality**,** due to defect and structural disorder.

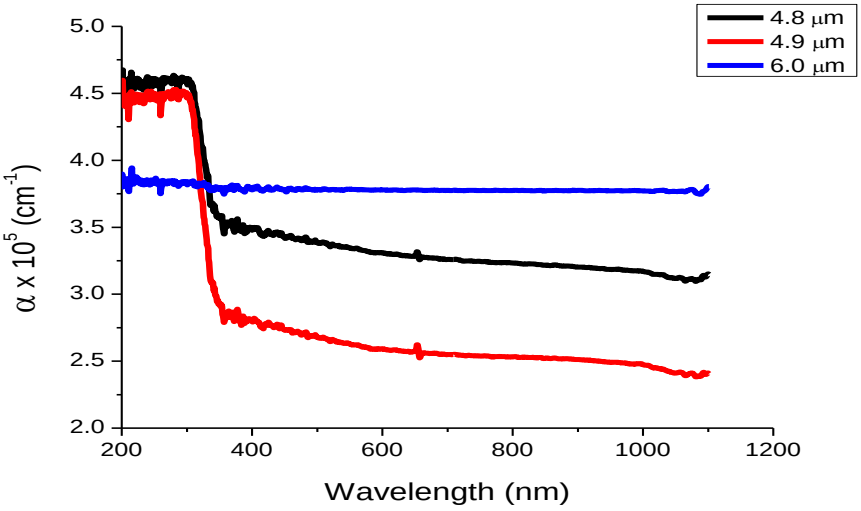

Figure 5. Plot of Absorption coefficient of SnO_2

The Urbach energy in **Figure 6(a)** is the region of weak absorption and was evaluated using Equation 10 (Bashar *et al*., 2019; Olasanmi *et al*., 2025). The equation can be compared with the linear expression "y = c + mx" where "m = $1/E_U$", and E_U equals 1,666 meV, 945 meV, and 12,210 meV for 4.8, 4.9, and 6.0 µm respectively. The SnO_2 of thickness 4.9 µm showed the optimal quality for optoelectronic application compared to 4.8 µm with slightly higher Urbach Energy. This is similar to the idea that the lowest thickness exhibits superior performance (Samantaray *et al*., 2021). On the contrary, the disorderliness in 4.8 µm thick film was more than that of 4.9 µm. Thus, 4.9 µm thick film have potential applications in photovoltaic absorbers with low efficiency, sensors, and thermoelectric devices.

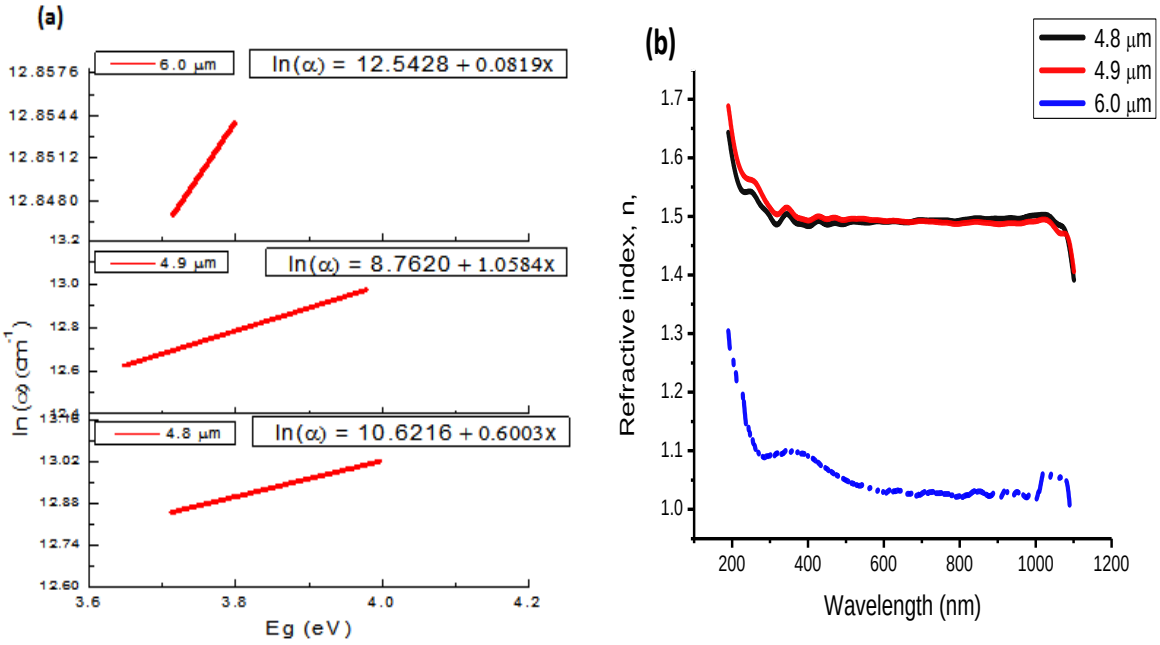

Figure 6. (a) Linear fitting of Urbach energy of ln(α) against Eg (b) Refractive index dispersion of SnO_2

For most semiconductors, Urbach energy increased with thickness (El Radaf and Hassanien, 2023). The high Urbach energy implies that the tin dioxide with 4.8 and 4.9 µm, should have low

carrier mobility, high recombination rate, and degradation with time. The 6.0 µm film thickness has a very high value of 12,210 meV which indicates complete insulation property. Factors that influence Urbach energy are strong ionic bonds, static disorder, thermal lattice vibrations, induced disorder, temperature, and average photon energies. Low Urbach energy is related with optimal optical and electronic properties, which makes a material important in thin films characterization (Ghasemi *et al*., 2022). It quantifies the level of disorderliness in the forbidden band gap zone.

The refractive index (RI) of optoelectronic materials is a crucial property, and its evaluation plays an essential role in the design of both linear and nonlinear optical devices (Polyansky, 2024). The refractive index values for 4.8–4.9 µm films are consistent with crystalline SnO_2 thin films, which are about1.5, showing normal dispersion. The 6.0 µm film exhibit abnormal lower refractive that is not expected of SnO_2 about 1.1. The abnormal refractive index of 6.0 µm film indicates defect-induced degradation, and it confirms that, increasing thickness beyond an optimum reduces optical quality (Nikiforov *et al*., 2020).

Conclusion

The green synthesis of SnO_2 using neem extract was successful and cheap. Tetragonal nanorods were obtained with diffraction peaks. The absorbance was noted to be very high with zero reflectance in the UV-Vis-IR regions. The green synthesis influenced the reduced values of energy band gap of 3.14 eV, 3.37 eV and 3.49 eV for 4.8, 4.9, and 6.0 µm respectively, compared to the known 3.6 eV. The threshold thickness for optimum optical quality was 4.9 µm. The zero reflectance of the SnO_2 obtained revealed the anti-reflectance property of the material. The transmittance and the refractive index were suitable for 4.8 and 4.9 µm, and the Urbach energy revealed their optoelectronics applications. The properties obtained brought the assertion that the 4.8 and 4.9 µm thick SnO_2 are suitable for optoelectronics with less efficiency, photovoltaic absorber and sensor.

Acknowledgement: We acknowledged the technical input of the Technologists of Physics Advanced Research Centre, SHESTCO.

Disclosure statement: *Conflict of Interest:* The authors declare that there are no conflicts of interest.
Compliance with Ethical Standards: This article does not contain any studies involving human or animal subjects.

References

Ali, J., Rehman, I. U., & Bangash, J. A. (2022). Phytochemicals content and in-vitro antioxidant properties of *Azadirachta indica* seeds, leaves and twigs prepared from different extraction techniques. *International Journal of Engineering, Science and Technology*, 14(4), 10–18. https://doi.org/10.4314/ijest.v14i4.2

Babalola, A. V., Oluwasusi, V., Owoeye, V. A., Emegha, J. O. *et al*. (2024). Effect of tin concentrations on the elemental and optical properties of zinc oxide thin films. *Heliyon*, 10(1), e23190. https://doi.org/10.1016/j.heliyon.2023.e23190.

Bashar, M. S., Matin, R., Sultana, M., Siddika, A., Rahaman, M., Gafur, M. A., & Ahmed, F. (2019). Effect of rapid thermal annealing on structural and optical properties of ZnS thin films fabricated by RF magnetron sputtering technique. *Journal of Theoretical and Applied Physics*, 13(4), 315–324. https://doi.org/10.1007/s40094-019-00361-5

Billur, C. A., Şahin, G., Güneri, E., Saatçi, B., & Soylu, M. Ç. (2020). The effect of film thickness on structural and optical properties of amorphous Sn_2O thin films deposited by inkjet printing method. *Journal of*

Molecular Structure, 1217, 128577. https://doi.org/10.1016/j.molstruc.2020.128577.

Bitu, M. N. A., Tanvir, N. I., Islam, S., & Farhad, S. F. U. (2023). Effect of substrate surface on the wide bandgap SnO_2 thin films grown by spin coating. *MRS Advances*, 8(10–11), 707–713. https://doi.org/10.1557/s43580-023-00515-3.

Chaves, A., Azadani, J. G., Alsalman, H., Da Costa, D. R., Frisenda, R., *et al*. (2020). Bandgap engineering of two-dimensional semiconductor materials. *NPJ 2D Materials and Applications*, 4, 29. https://doi.org/10.1038/s41699-020-00162-4.

Chen, H., Tan, C., Sun, D., Zhao, W., Tian, X., & Huang, Y. (2018). Ultrawide range tuning of direct band gap in Mg–ZnO monolayer via electric field effect. *RSC Advances*, 8(7), 3954–3961. https://doi.org/10.1039/C7RA11766A.

Drozdowska, K., Rehman, A., Krajewska, A., Lioubtchenko, D. V., Pavlov, K., *et al*. (2022). Effects of UV light irradiation on fluctuation enhanced gas sensing by carbon nanotube networks. *Sensors and Actuators B: Chemical*, 353, 131069. https://doi.org/10.1016/j.snb.2021.131069.

El Radaf, I. M., & Hassanien, A. S. (2023). Effect of thickness on structural, optical, and optoelectrical properties of sprayed $CuInSnS_4$ thin films as a new absorber layer for solar cells. *Physica B: Condensed Matter*, 657, 414867. https://doi.org/10.1016/j.physb.2023.414867

Eqbal, E., & Anila, E. I. (2021). Tailoring the properties of tin dioxide thin films by spray pyrolysis technique. *Optical Materials*, 115, 111653. https://doi.org/10.1016/j.optmat.2021.111653.

Ghasemi, B., Ševčík, J., Nádaždy, V., Végsö, K., Šiffalovič, P., Urbánek, P., *et al*. (2022). Thickness dependence of electronic structure and optical properties of F8BT thin films. *Polymers*, 14(3), 641. https://doi.org/10.3390/polym14030641.

Habte, A. G., Hone, F. G., & Dejene, F. B. (2022). Influence of Cu-doping concentration on the structural and optical properties of SnO_2 nanoparticles by co-precipitation route. *Journal of Nanomaterials*, 2022, 5957125. https://doi.org/10.1155/2022/5957125

Haq, S., Ahmad, P., Khandaker, M. U., Faruque, M. R. I., Rehman, W., Waseem, M., & Din, S. U. (2021). Antibacterial, antioxidant and physicochemical investigations of tin dioxide nanoparticles synthesized via microemulsion method. *Materials Research Express*, 8(3), 035014. https://doi.org/10.1088/2053-1591/abed8a

Kumar, A., Meunier-Prest, R., & Bouvet, M. (2020). Organic heterojunction devices based on phthalocyanines: A new approach to gas chemosensing. *Sensors*, 20(17), 4700. https://doi.org/10.3390/s20174700.

Kumar, K. J., Raju, N. R. C., & Subrahmanyam, A. (2011). Thickness dependent physical and photocatalytic properties of ITO thin films prepared by reactive DC magnetron sputtering. *Applied Surface Science*, 257(9), 4144–4149. https://doi.org/10.1016/j.apsusc.2010.10.119

Li, F., Liu, Q., Hu, J., Yang, J., & Ma, J. (2020). Recent progresses on SnO_2 anode materials for sodium storage. *Journal of Physics D: Applied Physics*, 53(26), 265501. https://doi.org/10.1088/1361-6463/ab8e79.

Liu, Q., Hu, Z., Chen, M., Zou, C., Wang, S., & Chou, S. L. (2019). Recent progress of layered transition metal oxide cathodes for sodium-ion batteries. *Small*, 15(10), 1805381. https://doi.org/10.1002/smll.201805381.

Meddas, H., Abdelghani, L., Amel, D., Saliha, B., Randa, S., Salah, A. M., & Okba, B. (2025). Elaboration of spin-coated deposition of tin oxide thin films: Effect of concentration. *Results in Optics*, 11, 100811. https://doi.org/10.1016/j.rio.2025.100811.

Miri, A., Sarani, M., Hashemzadeh, A., & Mardani, Z. (2018). Biosynthesis and cytotoxic activity of lead oxide nanoparticles. *Green Chemistry Letters and Reviews*, 11(4), 457–467. https://doi.org/10.1080/17518253.2018.1547926.

Nikiforov, A., Timofeev, V., Mashanov, V., Azarov, I., Loshkarev, I., & Volodin, V. (2020). Formation of SnO and SnO_2 phases during the annealing of SnO_x films obtained by molecular beam epitaxy. *Applied Surface Science*, 512, 145735. https://doi.org/10.1016/j.apsusc.2020.145735

Olasanmi, O. O., Akinsola, S. I., Aregbesola, E. A., Yusuf, K. A., Alabi, A. B., Ajani, D. A., & Omoniyi, F. O. (2025). Preparation of CuSe binary compound from Cu:Se thin films and its subsequent thermal annealing. *FUOYE Journal of Pure and Applied Sciences,* 10(1), AISC2886. https://doi.org/10.55518/fjpas.AISC2886

Omoniyi F. O., Omoteji I. B., Alu N., Imalerio T. I. (2025). Green Synthesis and Characterization of Lead (II) Oxide (PbO) Nanoparticles Using Neem Plant Extract as a Natural Reducing Agent. *EHEI-Journal of Science & Technology*, 5(1), 38-47. https://doi.org/10.34874/PRSM.ehei-jst-vol5iss1.62747

Oyelade, O. V., Idris, A.., Mohammed, M., Gimba, S., Felix, J. *et al* (2025). Green synthesis of some selected transition metal oxide nanoparticles for energy storage applications in supercapacitors. *Journal of the Indian Chemical Society*, 102(4), 101666. https://doi.org/10.1016/j.jics.2025.101666

Özmenteş, R. (2025). Role of thickness on the optical and electrical properties of physically evaporated TiO_2 thin films and silicon-based n-TiO_2/p-Si heterojunction configurations. *Journal of Materials Science: Materials in Electronics*, 36(1), 1039–1052. https://doi.org/10.1007/s10854-025-15153-8

Park, M. S., Kang, Y. M., Wang, G. X., Dou, S. X., & Liu, H. K. (2008). The effect of morphological modification on the electrochemical properties of SnO_2 nanomaterials. *Advanced Functional Materials*, 18(3), 455–461. https://doi.org/10.1002/adfm.200700407.

Polyanskiy, M. N. (2024). Refractive index info database of optical constants. *Scientific Data*, 11(1), 94. https://doi.org/10.1038/s41597-023-02898-2

Rafee, V., Razeghizadeh, A., Kazeminezhad, I., & Zalaghi, L. (2025). Effect of sol aging on the structural and optical properties of tin dioxide (SnO_2) nanoparticles and thin films. *Materials Science and Engineering: B*, 320, 118395. https://doi.org/10.1016/j.mseb.2025.118395

Samantaray, M. R., Gautam, P. K., Ghosh, D. S., & Chander, N. (2021). Spray deposited TiO_2 thin films for large-area TiO_2/p-Si heterojunction solar cells. *Engineering Research Express*, 3(1), 015043. https://doi.org/10.1088/2631-8695/ac41b6

Shen, W. (2012). Properties of SnO_2-based gas-sensing thin films prepared by inkjet printing. *Sensors and Actuators B: Chemical*, 166–167, 110–116. https://doi.org/10.1016/j.snb.2012.01.019.

Shin, S. W., Song, I. H., & Um, S. H. (2015). Role of physicochemical properties in nanoparticle toxicity. *Nanomaterials*, 5(3), 1351–1361. https://doi.org/10.3390/nano5031351.

pSutjaritvorakul, T., & Chutipaijit, S**.** (2020). Biological synthesis and characterization of lead oxide nanoparticles using *Averrhoa bilimbi* Linn. aqueous extract. *AIP Conference Proceedings*, 2279(1), 030003. AIP Publishing LLC. https://doi.org/10.1063/5.0023318.

Tazikeh, S., Akbari, A., Tabeli, A., & Tabeli, E. (2014). Synthesis and characterization of tin oxide nanoparticles via the co-precipitation method. *Materials Science-Poland*, 32(1), 23–28. https://doi.org/10.2478/s13536-013-0164-y

Waris A., Din M., Ali A., Ali M., Afridi S., Baset A., et al. (2021). A comprehensive review of green synthesis of copper oxide nanoparticles and their diverse biomedical applications. *Inorg. Chem. Commun.* 123, 108369. https://doi.org/10.1016/j.inoche.2020.108369